Spatial and temporal resolution of millennial scale geomagnetic field models

M. Korte [a] C.G. Constable [b]

[a] *GeoForschungsZentrum Potsdam, Telegrafenberg, 14473 Potsdam, Germany, monika@gfz-potsdam.de*

[b] *Institute of Geophysics and Planetary Physics, Scripps Institution of Oceanography, University of California at San Diego, La Jolla, CA 92093-0225, USA, cconstable@ucsd.edu*

Abstract

We assess the resolution and reliability of CALS7xK, a recently developed family of global geomagnetic field models. CALSxK are derived from archaeo- and paleomagnetic data and provide a convenient temporally varying spherical harmonic description of field behaviour back to 5000 BC. They can be used for a wide range of studies from gaining a better understanding of the geodynamo in the Earth's core to enabling the efficient determination of the influence of the geomagnetic field on cosmogenic nuclide productions rates. The models are similar in form to those derived from modern satellite observations, observatory and historical data, and used for the International Geomagnetic Reference Field, but their spatial and temporal resolution are limited by data quality and distribution. We find that spatial power is fully resolved only up to spherical harmonic degree 4 and temporal resolution is of the order of 100 years. Significant end effects associated with the temporal development in natural B-splines affect some features of the models in both the earliest and most recent century. Uncertainties in model predictions of declination,

inclination and field intensity in general are smaller than 2° and 1.5 μT respectively, but can be as large as 8° and 5 μT for certain regions and times. The resolution studies are complemented by a detailed presentation of dipole moment and dipole tilt as predicted by the model CALS7K.2. These largest scale features are resolved more reliably than complex details of the field structure and are useful, for example, in studies of geomagnetic cutoff rigidities of cosmogenic isotopes.

Key words: Geomagnetic field model, Dipole moment, Archaeomagnetism

1 Introduction

The geomagnetic field surrounds the Earth like a giant shield, influencing the path of the solar wind and the trajectories of solar particles and cosmic rays. At the Earth's surface, a dipole currently tilted by about 11° accounts for 90% of the observed geomagnetic field. The main part of the internal or core field, is caused by the geodynamo operating in the fluid outer core of the Earth. The region around the Earth which is influenced by the magnetic field is the magnetosphere, and electric currents flowing in various regions within the magnetosphere cause additional magnetic fields, the so-called external field contributions. The magnetosphere extends to about 10 Earth radii on the sunward side and is streched far out under the influence of the solar wind on the side away from the sun. Whether incoming particles can reach the atmosphere or not is determined by their energy and the geomagnetic field strength, which sets the geomagnetic cutoff rigidity. Only particles with energies above a certain level can penetrate the magnetic field and reach the atmosphere.

Models that describe the magnetosphere and near-Earth geomagnetic field

are used to study geomagnetic cutoff and cosmognic nuclide production rates. A series of such models has been developed by Tsyganenko and co-workers (Tsyganenko, 1995, 2000, 2002a,b; Tsyganenko et al., 2003; Tsyganenko and Sitnov, 2005) [1], describing the time-varying magnetosphere as a function of orientation of the magnetic dipole axis relative to the sun, solar activity and interplanetary magnetic field. In these models the geomagnetic main field is sometimes simply approximated by an axial dipole, but this is a crude assumption which might lead to significant errors in geomagnetic cutoff calculations. The dipole tilt and significant deviations from simple dipole symmetry in some regions of the Earth are not in general small enough to be considered negligible. These effects can be taken into account if geomagnetic main field models like the International Geomagnetic Reference Field (IGRF [2], (e.g. Macmillan et al., 2003)) are used. Main field models are based on a spherical harmonic representation where the field is described through the sum of the best-fitting tilted dipole (spherical harmonic degree 1) and more complex structure from higher spherical harmonic degrees.

Ice cores or rocks of the Earth's crust can contain isotopes which offer the possiblility to study past rates of nuclide production (mainly ^{10}Be, ^{14}C, ^{36}Cl), used to determine past solar irradiation rates and climate changes (e.g. Solanki et al., 2004). These nuclide production rates, however, are also influenced by the temporal variability of the geomagnetic field (e.g. Elsasser et al., 1956; Lal, 1988; Stuiver et al., 1991; Masarik and Beer, 1999; Muscheler et al., 2005). Dipole strength, dipole tilt and the more complex features of the geomagnetic field all change with time, but the first two clearly have the strongest influence

[1] http://nssdc.gsfc.nasa.gov/space/model/magnetos/data-based/modeling.html
[2] http://www.ngdc.noaa.gov/IAGA/vmod/igrf.html

on global production rates on the time scale of several thousand years. Changes of the geomagnetic field on the millennial time-scale, however, have not been known in much detail until recently. Virtual (axial) dipole moments (VDMs, VADMs) and virtual geomagnetic pole positions (VGPs) were used to describe the field evolution from the limited amount of archaeo- and paleomagnetic data available. A problem with these descriptions is that they cannot correctly account for contributions from the non-dipole field (VDMs, VGPs) or even the non-axial dipole field (VADMs). This leads to significant uncertainties in determining the geomagnetic dipole moment, and causes systematic errors of the kind shown by Korte and Constable (2005c) for VADM estimates of the past 7 kyrs (McElhinny and Senanayake, 1982; Yang et al., 2000). A further problem is that in attempts to minimize the influence of the more complex field contributions, VDMs and VADMs are usually averaged over periods of several centuries to a millennium, significantly limiting the temporal resolution of such dipole moment estimates.

With the advent of global paleofield modeling, more detailed studies of geomagnetic field behavior have become feasible. First attempts were made by Ohno and Hamano (1993) and Hongre et al. (1998). The limited global distribution of available data led them to truncate the spherical harmonic expansion at low degrees. While the data distribution limits the resolution of smaller spatial scales, a simple truncation of the series leads to spatial aliasing effects, i.e. mapping of power from more complex structure into dipole and quadrupole coefficients, thus affecting the reliability of even these strongest field contributions. Constable et al. (2000) were the first to expand the spherical harmonic series to higher degrees and apply regularisation techniques in the same way as used in models from current data to avoid spatial aliasing effects. The first

model only consisted of snapshots every 100 years for the past 3000 years, but in the meantime this family of models has been improved first by using a description that is continuous in time (CALS3K.1 (Korte and Constable, 2003)), then constraining the models by a larger amount of data (CALS3K.2) and extending them further back in time. The latest version is CALS7K.2 covering the time span from 5000 BC to 1950 AD (Korte and Constable, 2005b) and further extensions to 10 kyr seem feasible (Korte and Constable, 2005d).

Here we summarize the general characteristics of the CALSxK family of models and the particular properties of the latest version, CALS7K.2. We present uncertainty estimates for model predictions, discuss limitations of the model for various applications and show the evolution of dipole moment strength and tilt as predicted by the model.

2 The model

2.1 Data and method

The name CALSxK.n stands for Continuous models of Archeomagnetic and Lake Sediment data for the past x kyrs, with the version number of the model indicated by the integer n. CALSxK models are constructed entirely from paleomagnetic data, which overlap temporally with systematic direct observations of geomagnetic field directions for about 400 years (Jonkers et al., 2003) and with absolute field intensity for less than 200 years (Gauss, 1839). Although it might be argued that a superior field model could be constructed by combining both historical and paleofield data, the exclusion of historical observations allows them to be used in an important check on the validity of

CALSxK against relatively high quality data for 1590-1950 AD.

The indirect paleomagnetic archives are provided by archeological materials, lavas, and sediments which acquired and preserved a magnetisation related to the geomagnetic field at some time in the past. In hot lava or clay, which is fired to form bricks or vessels, the magnetic moments associated with ferromagnetic minerals in the material preferentially align with the ambient geomagnetic field. This magnetisation is "frozen in" when the material cools below the Curie-temperature of the magnetic minerals, acquiring a thermoremanent magnetisation. During sedimentation, magnetic grains are preferentially aligned with the geomagnetic field during the depositional process, and become locked in position when the sediment turns to rock (detrital remanent magnetisation). Declination and inclination of the past field can be determined from oriented samples of such materials. Obtaining information about past field intensity is more difficult. The magnetisation of material with thermoremanent magnetisation can be proportional to the field intensity, and this intensity can be recovered in laboratory experiments using one of many variants on the Thellier (1941) technique (e.g. Coe et al., 1978; Shaw, 1974; Riisager and Riisager, 2001) or the more recently adopted microwave approach (Walton et al., 1993). These kinds of determinations provide estimates of the absolute intensity of the past field. This cannot be achieved from sediments. Fluctuations in the magnetisation of the sediments with time may be due to variations in field intensity, but are also influenced by lithology and concentration of magnetic material. Careful normalisation can produce a record of past relative field intensity variations, but information on absolute field strength requires independent calibration. For this reason sediment intensity data were not used in CALS7K.2 and earlier models.

In the first version of the model (CALS3K.1) we used no intensity data at all, but only declination and inclination. The development of the axial dipole was prescribed in the model to scale it to an appropriate field strength, and we used a template based on linear interpolation of the VADMs published by Yang et al. (2000). Consequently, this particular model provides no independent estimate of the dipole moment. The data used in CALS3K.1 were limited to 24 smoothed time series of observations reduced to common locations. In all subsequent models we used the data as they were published; for archeomagnetic data this means that there are no time series from individual locations and the data are scattered both in space and time. CALS3K.2 was the first model to include archeointensity data together with directional data and this model and the subsequent 7 kyr models provide a dipole moment estimate directly from the data. The data distribution is far from even (Fig. 1). While many data are available from the European region, sampling in the Southern hemisphere is particularly sparse. Similarly, the temporal data distribution is quite variable as can be seen in Fig. 2. The amount of global data increases significantly for epochs younger than about 1000 BC. The total number of data for the individual geomagnetic elements is listed in Table 1.

Our modelling method follows the approach used by Bloxham and Jackson (1992) and Jackson et al. (2000) for their century scale models. It is based on a spherical harmonic expansion in space, with the continuous temporal representation provided by expanding each Gauss coefficient in a cubic B-spline representation in time. With the approximation of an insulating mantle, and neglecting crustal fields and external fields the time-dependent geomagnetic main field $\mathbf{B}(\mathbf{t})$ is described as the gradient of a scalar potential $V(t)$, that is

$$\mathbf{B}(\mathbf{t}) = -\nabla \mathbf{V}(\mathbf{t}) \tag{1}$$

everywhere outside the source region in Earth's core:

$$V(r,\theta,\phi,t) = a\sum_{l=1}^{L}\sum_{m=0}^{l}\sum_{k=1}^{K}\left(\frac{a}{r}\right)^{l+1}[g_l^{m,k}\cos(m\phi)+h_l^{m,k}\sin(m\phi)]P_l^m(\cos\theta)M_k(t) \qquad (2)$$

where (r,θ,ϕ) are spherical polar coordinates and $a = 6371.2$km is the mean radius of the Earth's surface. The $P_l^m(cos\theta)$ are the Schmidt quasi-normalised associated Legendre functions of degree l and order m. The coefficients $\{g_l^{m,k}, h_l^{m,k}\}$ are related to the standard Gauss coefficients $\{g_l^m, h_l^m\}$ for a single epoch t by

$$g_l^m(t) = \sum_{k=1}^{K} g_l^{m,k} M_k(t) \qquad (3)$$

and the same for h_l^m. Cubic B-splines are piecewise cubic polynomials, which form a basis of minimal support (de Boor, 1978). The ith cubic B-spline M_i is nonzero ($M_i(t) > 0$) only if t lies in the interval $[t_i, t_{i+4}]$ of knot points t_k, $k = 1$ to K. Equally spaced knot points are used here, and extra knot points extend beyond the boundaries of the model. The influence of this choice on behavior near the ends of the model is discussed further in Section 2.3.

Both the maximum degree and order of the spherical harmonics and the knot-point spacing of the splines are chosen to allow for better resolution than we can expect from the data, ensuring that the structure of the model will not be limited by the truncation levels specified by L and K. Instead, a physically motivated regularization is used to ensure smoothness and simplicity of the model at times and places where the data cannot provide high resolution. The model is determined from a trade-off among fit to the data, smooth spatial structure of the field by minimising the heat-flow at the core-mantle boundary and a smooth development in time by minimising the second time derivative of the field. For our preferred models we choose the misfit level for the data

as the expected value chi-squared based on the estimated uncertainties, which we tried to determine in a coherent way for all kinds of data based on our understanding of their possible errors. Details of modelling method and error estimates are described in Korte and Constable (2003); Korte et al. (2005); Korte and Constable (2005b). Note that while in CALS3K.1 the axial dipole was not directly determined from the data but prescribed as a scaling factor, in the later models it is obtained directly from all data including intensity measurements. Consequently, the later models provide an independent estimate for the dipole moment without a priori information.

2.2 Spatial resolution

The CALSxK models can provide field predictions for any location and time within their valid age span, but for several reasons the actual spatial and temporal resolution, i.e. the accuracy, are much lower than in models from current data. The inhomogeneous and incomplete global data coverage limits the spatial resolution and, even with perfectly accurate data, this means we could not expect to resolve spherical harmonic degrees higher than 6 (Korte and Constable, 2005d). However, it should be obvious from the earlier brief description of the mechanisms for magnetic remanence acquisition that archeo- and paleomagnetic data contain very large uncertainties compared to direct field measurements. Alterations of the initial magnetisation might have occurred over time, for directional data, the orientation of the samples is never exact, inclination flattening (effectively an inaccurate recording of the field direction) might have occured in sediments, to name just a few possible sources of errors. One of the most severe problems is determining the age of

magnetization. Archaeologists might be able to tell the age of a sample within an uncertainty of a few years, and a similar accuracy is sometimes achieved for sediments dated by varve counting. In general, however, even archaeologically dated material will have age uncertainties on the order of decades, and this is also true for material dated by radiocarbon. Some age uncertainties are as large as a few centuries, a severe limitation on temporal resolution of the model.

We chose degree and order 10 as truncation level for the spherical harmonic expansion and a knot-point spacing of 55 years. A comparison of the spatial power spectrum of the CALSxK models with models from current data give an idea of the actual spatial resolution of the models (Fig. 3a). The first few degrees, i.e. the dipole, quadrupole and octupole contributions, agree very well among the models. However, we see a drop-off in power starting at degree 8 or 9 in the 400-year model GUFM1 when compared with POMME 1.4. The latter is based on satellite data (Maus et al., 2005), and has full spatial resolution of the core field out to spherical harmonic degree 13-15 where it is overwhelmed by the crustal field. The absence of power in GUFM1 reflects the influence of the model regularization on the higher degrees, (i.e., the smaller scale structure) and the limits on actual spatial resolution. In the CALSxK models, not surprisingly the drop-off starts already around degree 4 or 5, due to the much higher data uncertainties and worse global data coverage. We conclude that we can resolve the first few degrees reliably but lose resolution around spherical harmonic degree 4, roughly equivalent to a spatial wavelength of 10000 km. A comparison of secular variation spectra (Fig. 3b) shows that the millennial scale models have less secular variation power in all the coefficients, which means that even the variations on large spatial scales, e.g. like the dipole

moment variation, are not fully resolved in time.

2.3 Temporal resolution

The discussion of the previous section is complicated somewhat by comparisons among models that span a range of time scales, and can be expected to have different temporal as well as spatial resolution. In this section we take up the question of temporal resolution, as it is of considerable importance in model applications.

For the purposes of illustration we begin with the representation of an arbitrary function $p(t)$ in terms of cubic smoothing splines, which in the context of CALSxK modelling can be thought of as representing the temporal evolution of a single Gauss coefficient (cf. Eq. 3). We write

$$p(t) = \sum_{k=1}^{K} \beta_k M_k(t) \tag{4}$$

where the M_k are cubic B-spline basis functions. In this one-dimensional problem the objective function minimized in finding $p(t)$ from data $(t_i, y_i), i = 1, \ldots, n$ on time interval (t_s, t_e) is

$$\sum_{i=1}^{n} (y_i - p(t_i))^2 + \tau \int_{t_s}^{t_e} [p''(t)]^2 dt \tag{5}$$

Figure 4(a) shows what the B-spline basis functions would look like for the time interval 1000-2000 AD for CALS7K.2. Note that the extension of the basis past 1950 AD (the end of the model interval) enforces a natural spline with $p''(t) = 0$ at t_e.

As noted in Section 2.1, the B-Splines form a basis with local support, and this

is convenient for computational purposes in deriving the model. However, the curve-fitting procedure has an equivalent representation as a variable kernel smoother convolved with the data - valid except near ends of interval. That is we can write (Silverman, 1984; Constable and Parker, 1988)

$$\hat{p}(s) = n^{-1} \sum_{i=1}^{n} G(t_i, s) y_i \tag{6}$$

with

$$G(s,t) = \frac{1}{f(t)h(t)} \kappa \left(\frac{s-t}{h(t)} \right) \tag{7}$$

$h(t)$ is the local bandwidth of the equivalent kernel, and $f(t)$ is the local density of knot points.

$$\kappa(u) = \frac{1}{2} \exp \left(-\frac{|u|}{\sqrt{2}} \right) \sin \left(\frac{|u|}{\sqrt{2}} + \pi/4 \right) \tag{8}$$

$h(t)$ can be discovered once the fit has been performed and τ is known.

$$h(t) = \left[\frac{\tau}{n f(t)} \right]^{\frac{1}{4}} \tag{9}$$

τ controls the tradeoff between smoothness in $p(t)$ and fitting the data. Note that the distance from the central peak to the first zero of $\kappa \approx 3.32h$. The function $G(s,t)$ can be thought of as the impulse response of a single datum in the fitting procedure; thus its bandwidth h is directly related to the temporal resolution of the model.

Near the boundary of the interval the representation for the kernel is a bit more complicated (Silverman, 1984). For any point $t \in [t_s, t_e]$ we define

$$\delta = \min(t - t_s, t_e - t) \tag{10}$$

as the distance from t to the nearest boundary. We want to find the equivalent kernel when δ is small. Define r and α, both depending on t and λ as

$$r\cos\alpha = 1 - 2\sin(\frac{\sqrt{2}\delta}{h}) \qquad\qquad r\sin\alpha = 1 - 2\cos(\frac{\sqrt{2}\delta}{h}) \tag{11}$$

and a kernel $\kappa^*(u)$ also implicitly dependent on t and λ by

$$\kappa^*(u) = -\frac{1}{\sqrt{8}}\exp\left(-\frac{|u|}{\sqrt{2}}\right)\sin\left(\frac{|u|}{\sqrt{2}} - \alpha\right). \tag{12}$$

Now let t^* be the reflection of t in the nearest boundary, that is

$$t^* = \begin{cases} t - 2\delta & \text{if } t < \frac{1}{2}(t_s + t_e) \\ t + 2\delta & \text{if } t > \frac{1}{2}(t_s + t_e) \end{cases} \tag{13}$$

Then for s and t in $[t_s, t_e]$

$$G(s,t) \equiv \frac{1}{f(t)h(t)}\left\{\kappa\left(\frac{s-t}{h(t)}\right) + \kappa^*\left(\frac{s-t^*}{h(t)}\right)\right\}. \tag{14}$$

The shape of this convolving kernel and how it changes on approaching the boundary t_e is illustrated in Fig. 4(b) for a local bandwidth $h = 50$ years.

The equivalent kernel representation provides a means of evaluating h after the fit is performed. But this description technically only applies for a smoothing spline with a knot at every data point, while our fitting procedure makes use of a depleted set of knots and an approximation to a smoothing spline. Constable and Parker (1988) give details about the nature of the approximation, and argue that it is reasonable provided the knot spacing, Δ, is chosen so that $\Delta < 1.65h$. For CALS7K.2 we used Δ of 55 years: accordingly we can expect reliable results with this depleted basis if $h > 33$ years. Users may prefer to think in terms of the distance from the central peak to the first zero crossing

for κ, here designated h_z. The minimum h_z is then $3.32h$, around 100 years. Loosely speaking we see that by this most optimistic measure the kernel would average data in a window about 2 centuries wide; otherwise the approximation to a smoothing spline will be poor. In fact we expect h to be wider than this minimum, because large uncertainties in many of the observations enforce a smoother model. The exact calculation of h for CALS7K.2 is complicated for a number of reasons: different weights are applied to individual data in the modeling; the temporal distribution of the observations is uneven so that h will vary along the time interval; and the geomagnetic elements are non-linearly related to the model parameters. There is also the influence of spatial smoothing to consider. However, empirical trials suggest that an appropriate average value for $h \approx 50$, making $h_z \approx 150$ years, and the resulting model an average over several centuries, but weighted strongly towards the center of the kernel. Temporal power spectral estimates for the individual Gauss coefficients (Korte and Constable, 2005a) support this interpretation.

The behavior of $G(s,t)$ seen in Fig. 4(b) near the end of the model interval is a cause for some concern which we will return to later. Far from the boundary, the kernel shape is symmetric about the vertical line indicating the nominal time t, but by 1800 AD it is apparent that data to the left of t inevitably have a stronger influence on the model fit than those lying to the right. We also see in Fig. 2, that there is a rapid drop in the number of data after 1800 AD, particularly in directional observations. This contributes to an effective broadening of the local bandwidth for the averaging kernel in line with Eq. 9, and some temporal bias in the resulting model.

We could obtain formal statistical uncertainty estimates for the coefficients from the modelling process, but such estimates are not very reliable given the high data uncertainties, uneven data distribution, and non-linear modeling scheme. To get a better idea about the reliability of the model we used a bootstrap technique: Based on the dataset underlying CALS7K.2, 3000 datasets with an identical number of data randomly drawn from the original set were created and modelled with the same parameters and numbers of iterations as for the original model. We used the results to determine the mean and standard deviation for all model coefficients and times.

From these 3000 bootstrap models we also predicted the values of declination, inclination and intensity on a grid of 10x10 degrees in latitude and longitude every 100 years in time and calculated the standard deviation for each time and grid point. The mean and maximum standard deviation values over the whole time span from 5000 BC to 1950 AD provide an estimate of uncertainties in model predictions for different regions (Fig. 5). For declination these are large at high geomagnetic latitudes as might be expected from its geometrical variation with latitude. Otherwise, except for a region from Southern Africa to Antarctica the mean standard deviation is less than about 2°. In inclination an area of high uncertainty in the southern Atlantic and northern Indian Ocean is obvious; these are connected to sparse and possibly problematic data from Africa. While for declination and inclination in general the uncertainties are smaller in areas with good data coverage, this is not true for intensity. On the contrary, apart from an area of high uncertainty in the South Pacific, the maximum uncertainties are largest in Europe and Asia, the areas with highest

intensity data coverage. This probably reflects the high uncertainties (average data uncertainty in B is 11 μT) and internal inconsistencies among intensity data, making the model quite sensitive to individual data in these regions. It also suggests that the low uncertainties in other regions may simply be a reflection of sparse data coverage concealing any such regional inconsistencies, so that the scale of intensity variations is muted by the model regularization. It remains to be seen whether using only high quality intensity data in models of this kind can substantially improve their resolution and accuracy.

The maximum standard deviations in Fig. 5 highlight regions where the model performs badly, but convey nothing about the timing of these maximum uncertainties, which are mostly confined to a few decades or centuries. The temporal variations of the standard deviations in the individual coefficients up to degree and order 4 are displayed in Fig. 6, which shows that there are some periods of higher general uncertainty for a few centuries, particularly around 4000 BC, 1200 BC, 100 AD and 900 AD. It is also notable that the uncertainties rise rapidly near the end points of the model span, suggesting that we might expect less satisfactory behavior in these time intervals.

3 Dipole variations and their reliability

There are many possible applications for the CALSxK, but their individual viability will depend on the reliability of the model, and as we have seen in Section 2 this depends on location, the time intervals of interest, and the spatial resolution desired. Figure 6 shows that the percentage uncertainties for the degree one terms are generally low, and in this section we discuss variations in the dipole moment and position of the dipole axis in the CALS7K.2 model.

The dipole moment estimate M, derived from the degree 1 spherical harmonic coefficients g_1^0, g_1^1 and h_1^1 as

$$M = \frac{4\pi}{\mu_0} a^3 \sqrt{(g_1^0)^2 + (g_1^1)^2 + (h_1^1)^2}, \tag{15}$$

with $a = 6371.2$ km the average radius of the Earth and $\mu_0 = 4\pi \cdot 10^{-7}$H/m, the permeability of free space, should be one of the most reliable features of the model. Reflecting the general global field strength, it is of interest for several purposes, from studying the geodynamo process deep inside the Earth to estimating the geomagnetic cutoff of cosmogenic nuclides produced in space. The predicted dipole moment evolution, together with its derivative reflecting the variability, is displayed in Fig. 7. The dipole moment is significantly weaker than previous VADM estimates, which have been shown to be biased systematically high (Korte and Constable, 2005c). The new dipole moment estimate is also considerable better resolved than previous estimates as can be seen in Fig. 8, which compares the resolution of the traditional VADM block averages in time with that achieved by CALS7K.2. The dipole moment shows rather strong variations down to centennial scales, but the comparison with GUFM confirms that although the two estimates agree within the estimated uncertainties for CALS7K.2, the paleofield model is unable to resolve high frequency changes seen in the historical record. In Korte and Constable (2005a) we have shown that the long term variations are robust. The rate of dipole moment change is not correlated with its magnitude. The bootstrap error in dipole moment estimate is about 3% on average, slightly higher for the earliest two millennia, clearly lower for the most recent millennia and particularly high

around 3900 BC (up to 7.7%) and 1000 BC (up to 5.5%). These uncertainties are not correlated with dipole moment magnitude, but tend to be larger during periods of rapid change. It is perhaps not obvious from Fig. 7, but they rise near the beginning and end of the model span, as should be anticipated in light of the discussion in Section 2.3.

3.2 Dipole tilt

The tilt of the dipole field contribution has also changed significantly over the past few millennia. Figure 9 shows the northern geomagnetic pole (i.e. dipole axis) position through time. For better time resolution the changes in latitude and longitude of the northern pole position are displayed individually in Fig. 10. Between 5000 BC and 3000 BC the pole displays a rather regular swing south and back north in a longitude range between 225 and 320°. This coincides with the time of low dipole moment. During the increase and phase of high dipole moment the geomagnetic pole movement is weaker, but involves almost all longitudes. With the decrease of dipole strength, however, the dipole tilt increases again, and returns to approximately the same longitudinal range as observed in the beginning of the studied time interval.

Also plotted in blue on Figs. 9 and 10 are estimates of average virtual geomagnetic pole (VGP) positions at l00 year intervals derived directly from the geomagnetic directional data (where both D and I were measured simultaneously), and in red predictions for the same data locations for CALS7K.2. Average VGP positions have often been used as a proxy for the location of the dipole axis, in much the same way as VADM is used for the dipole moment. In general the VGPs predicted from CALS7K.2 agree well with the VGPs

derived from the data, but at some times there are substantial differences between the VGPs and the actual dipole axis location for CALS7K.2. As might be expected, the largest differences are coincident with the times of greatest non-dipole field contributions (see Fig. 8 of Korte and Constable (2005c)).

To check the reliability of these dipole tilt estimates, we compared them to those from the historical GUFM model (Jackson et al., 2000), covering the epochs from 1590 to 1990 from historical data (gray line on Fig. 10). Note that the axial dipole strength in GUFM has been extrapolated back from 1830, as no direct measurements of intensity are available for earlier epochs. However, this extrapolation should not significantly affect the dipole tilt determined by the non-axial parts of the dipole. Between 1590 and about 1800 AD predictions from GUFM and CALS7K are in reasonable agreement, and the GUFM dipole longitudes lie within the (admittedly broad) 95% confidence limits for CALS7K.2 throughout the 400 year time interval. The same is not true for the latitudes: it seems that CALS7K.2 systematically over-estimates the dipole latitude, although the differences only become really noticeable after 1800AD when the general trend is different for the two models. The CALS7K estimate lies closer to the VGPs, but GUFM has higher spatial and temporal resolution and must be assumed to give the more reliable estimate. We suppose that in this time interval CALS7K.2 is contaminated by the end effects discussed in Section 2.3. These seem particularly acute because of the rapid decrease in the number of directional data contributing to the model between 1800 and 1950 AD. We were able to verify this interpretation by remaking the CALS7K.2 model on a truncated time interval, terminating at 1800 AD. In the truncated model there was also an end effect, although the influence on the model was less pronounced because the number of directional data remained

high near the interval boundary.

4 Discussion and Conclusions

We have presented a review of recent progress in describing the global geomagnetic field evolution of the past 7 kyr, up to the latest model CALS7K.2. Data and modeling methodology have been summarized and and improved estimates of both temporal and spatial accuracy of the model have been given. Due to limited data coverage and large uncertainties in the data only the first 3 to 4 spherical harmonic degrees can be resolved, and the reliability of the model varies with both time and place. Studies of the temporal resolution suggest that on average it can be no better than about 100 years, and in sparsely sampled regions and at smaller spatial scales the model averages over several centuries.

The CALS7K model provides a revised estimate of past dipole moment evolution, offering improved temporal resolution and more reliable absolute field strength estimates than previous VADM studies. The absolute dipole strength has been overestimated by VADMs, but the relative magnitude of millennial-scale variation is confirmed by the global model; the maximum between 1000 BC and 1000 AD is larger by a factor of 1.8 than the minimum between 5000 BC and 3500 BC. Comparisons with historical field models show that there are short term variations (less than a century) which remain unresolved. The variation of geomagnetic pole position with time suggests that the dipole tilt is larger at times of low dipole moment. Poor agreement between pole positions for CALS7K.2 and GUFM in very recent times can be attributed at least in part to the use of natural splines for the temporal development: these are con-

strained to have zero second derivatives at the interval boundary. The rapid fall-off in number of paleofield data for the most recent century is also a contributing factor. The use of more appropriate end conditions should improve this in future modeling efforts.

Our motivation in developing these models was to extend the time scales of global models describing the main field evolution. From the 400 year model of GUFM we know for example that the anomalous weak field in the South Atlantic and weak secular variation in the Pacific area compared to the rest of the world have been in existence for several centuries. Two prominent flux lobes, areas of high concentration of magnetic flux at the core-mantle boundary (CMB) appear persistent over the whole time interval (Jackson et al., 2000). The geomagnetic dipole moment has been decreasing with a speed significantly faster than the free decay of the field expected if the dynamo were switched off when observations of field intensity began 170 years ago (Olson, 2002). The longevity of all these features is unconstrained by the historical models and the CALSxK models provide a tool for studying them on millennial timescales. It is now clear that the current dipole decay is far from monotonic when considered on the 0-7 ka time interval. The nature of the South Atlantic anomaly remains ambiguous, in large part because the model is least accurate in this region.

Theories have been developed about processes in the core in attempts to explain secular variation and particularly the very abrupt changes named geomagnetic jerks. Studying jerks would require better resolution than will ever be feasible from paleodata, but the model may be useful to test for the existence of torsional oscillations (Bloxham et al., 2002) or MAC (magnetic, Archimedes, Coriolis) waves (Braginsky, 1967; Finlay and Jackson, 2003) in

the core on longer timescales. It is expected that the role of diffusion in the core will have to be more fully explored as we move to interpret longer time scale secular variations. For all these applications it is clearly important to keep in mind the limitations in spatial and temporal resolution of the models.

The CALSxK models will also be useful in comparisons to dynamo simulations, which seem able to describe some of the features observed in the geomagnetic field quite well, but may be lacking in other important characteristics. The true relevance of dynamo models is sometimes placed in doubt because some of their parameters are still far from those estimated for Earth (Dormy et al., 2000). Results from data-based models may provide useful additional constraints on such numerical models.

A further application of the models is as a calibration tool for relative paleointensity data series (Korte and Constable, 2005d). It can be shown from simple comparison to model predictions that if the relative intensity data are suitably normalised a constant calibration factor seems suitable for whole time series. This opens the possibility of extending the CALSxK models further back in time, as the present 7 kyr limit is mainly due to the extreme scarcity of absolute archeointensity data prior to 5000 BC. Sediment time series are often significantly longer. With the assumption that calibration factors determined from 7 kyrs are valid also for 10 or 12 kyrs we will have enough intensity data to attempt global models for such time spans.

There remains substantial scope for improvement in millennial scale field models. Improved modeling strategies should give better agreement with historical observations and models. Promising results from a study on relative intensity data from sediments and the continuing publication of new archeo- and high

resolution Holocene paleomagnetic results suggest that an extension of the existing models to 10 kyr will soon become feasible.

5 Resources for users

The CALSxK models are described by sets of spherical harmonic coefficients at each knot-point of the temporal splines. The models are available on the internet together with FORTRAN77 programs to evaluate them. The programs, which can be modified for individual needs as the source code is available provide spherical harmonic coefficient sets for individual times just like the IGRF coefficients, predictions of the geomagnetic field components at the Earth's surface for any time and location or whole time series of field evolution at individual locations. The material can be found at http://www.gfz-potsdam.de/pb2/pb23/Models/CALS7K/index.html and http://mahi.ucsd.edu/cathy/Holocene/CALS
as well as in the EarthRef Digital Archive (ERDA) at http://earthref.org where the search function with the respective models' name will give the desired result.

References

Bloxham, J., Jackson, A., 1992. Time-dependent mapping of the magnetic field at the core-mantle boundary. J. Geophys. Res. 97, 19,537–19,563.

Bloxham, J., Zatman, S., Dumberry, M., 2002. The origin of geomagnetic jerks. Nature 420(6911), 65–68.

Braginsky, S., 1967. Magnetic waves in the Earth's core. Geomagn. Aeron. 7, 851–859.

Coe, R., Gromme, S., Mankinen, E., 1978. Geomagnetic paleointensities from radiocarbon-dated lava flows on Hawaii and question of Pacific nondipole low. J. Geophys. Res. 83, 1,740–1,756.

Constable, C., Johnson, C., Lund, S., 2000. Global geomagnetic field models for the past 3000 years: transient or permanent flux lobes? Phil. Trans. R. Soc. Lond. A 358, 991–1008.

Constable, C. G., Parker, R. L., 1988. Smoothing, splines and smoothing splines: Their application in geomagnetism. J. Comput. Phys. 78, 493–508.

de Boor, C., 1978. A Practical Guide to Splines. Springer-Verlag, New York.

Dormy, E., Valet, J.-P., Courtillot, V., 2000. Numerical models of the geodynamo and observational constraints. Geochem., Geophys., Geosys. 1, doi:10.1029/2000GC000062.

Elsasser, W., Ney, E., Winckler, J., 1956. Cosmic-ray intensity and geomagnetism. Nature 178, 1226–1227.

Finlay, C., Jackson, A., 2003. Equatorially dominated magnetic field change at the surface of Earth's core. Science 300, 2084–2086.

Gauss, C., 1839. Allgemeine Theorie des Erdmagnetismus. In: Resultate aus den Beobachtungen des des magnetischen Verein im Jahre 1838. Göttinger Magn. Ver., Leipzig, pp. 1–52.

Hongre, L., Hulot, G., Khokhlov, A., 1998. An analysis of the geomagnetic field over the past 2000 years. Phys. Earth Planet. Interiors 106, 311–335.

Jackson, A., Jonkers, A., Walker, M., 2000. Four centuries of geomagnetic secular variation from historical records. Phil. Trans. R. Soc. Lond. A 358, 957–990.

Jonkers, A., Jackson, A., Murray, A., 2003. Four centuries of geomagnetic data from historical records. Rev. Geophys. 41.

Korte, M., Constable, C., 2003. Continuous global geomagnetic field models

for the past 3000 years. Phys. Earth Planet. Interiors 140, 73–89.

Korte, M., Constable, C., 2005a. Centennial to millennial geomagnetic variation, submitted to GJI.

Korte, M., Constable, C., 2005b. Continuous geomagnetic field models for the past 7 millennia: 2. CALS7K. Geochem., Geophys., Geosys. 6, Q02H16, doi:10.1029/2004GC000801.

Korte, M., Constable, C., 2005c. The geomagnetic dipole moment over the last 7000 years - new results from a global model. Earth Planet. Sci. Let. 236, 348–358.

Korte, M., Constable, C., 2005d. How relative paleointensity records and intensity data distribution can improve global millennial scale geomagnetic field models, submitted to G3.

Korte, M., Genevey, A., Constable, C., Frank, U., Schnepp, E., 2005. Continuous geomagnetic field models for the past 7 millennia: 1. a new global data compilation. Geochem., Geophys., Geosys. 6, Q02H15, doi:10.1029/2004GC000800.

Lal, D., 1988. Theoretically expected variations in the terrestrial cosmic-ray production rates of isotopes. In: Castagnoli, G. C. (Ed.), Solar-Terrestrial Relationships and the Earth Environment in the Last Millennia. North-Holland Physics Publishing, Amsterdam, pp. 216–233.

Macmillan, S., Maus, S., Bondar, T., Chambodut, A., Golovkov, V., Holme, R., Langlais, B., Lesur, V., Lowes, F., Lühr, H., Mai, W., Mandea, M., Olsen, N., Rother, M., Sabaka, T., Thomson, A., Wardinski, I., 2003. The 9th-generation Iinternational Geomagnetic Reference Field. Geophys. J. Int. 155, 1051–1056.

Masarik, J., Beer, J., 1999. Simulation of particle fluxes and cosmogenic nuclide production in the Earth's atmosphere. J. Geophys. Res. 104, 12,099–

12,111.

Maus, S., Lühr, H., Balasis, G., Rother, M., Mandea, M., 2005. Introducing POMME, the POtsdam Magnetic Model of the Earth. In: Reigber, C., Lühr, H., Schwintzer, P., Wickert, J. (Eds.), Earth Observation with CHAMP - Results from Three Years in Orbit. Springer Verlag, Berlin, pp. 293–298.

McElhinny, M., Senanayake, W., 1982. Variations in the geomagnetic dipole: I. The past 50 000 years. J. Geomag. Geoelectr. 34, 39–51.

Muscheler, R., Beer, J., Kubik, P., Synal, H.-A., 2005. Geomagnetic field intensity during the last 60,000 years based on ^{10}Be and ^{36}Cl from the Summit ice core and ^{14}C. Quatern. Sci. Rev. 24, 1849–1860.

Ohno, M., Hamano, Y., 1993. Spherical harmonic analysis of paleomagnetic secular variation curves. Central Core of the Earth 3, 205–212.

Olson, P., 2002. The disappearing dipole. Nature 416, 591–594.

Riisager, P., Riisager, J., 2001. Detecting multidomain magnetic grains in Thellier palaeointensity experiments. Phys. Earth Planet. Inter. 125, 111–117.

Shaw, J., 1974. A new method of determining the magnitude of the palaeomagnetic field; application to five historic lavas and five archaeological samples. Geopys. J. R. Astr. Soc. 39, 133–141.

Silverman, B., 1984. Spline smoothing: the equivalent variable kernel method. The Annals of Statistics 12, 898–916.

Solanki, S., Usoskin, I., Kromer, B., Schüssler, M., Beer, J., 2004. Unusual activity of the sun during recent decades compared to the previous 11,000 years. Nature 431, 1084–1087.

Stuiver, M., Braziunas, T., Becker, B., Kromer, B., 1991. Climatic, solar, oceanic, and geomagnetic influence on Late-Glacial and Holocene atmospheric ^{14}C/^{12}C change. Quatern. Res. 35, 1–24.

Thellier, E., 1941. Sur la vérification d'une méthode permettant de déterminer l'intensité du champ terrestre dans le passé. C. R. Hebd. Seances Acad. Sci. 212, 281–283.

Tsyganenko, N., 1995. Modeling the earth's magnetospheric magnetic field confined within a realistic magnetopause. J. Geophys.Res. 100, 5599–5612.

Tsyganenko, N., 2000. Modeling the inner magnetosphere: The asymmetric ring current and region 2 birkeland currents revisited. J.Geophys.Res. 105, 27739–27754.

Tsyganenko, N., 2002a. A model of the near magnetosphere with a dawn-dusk asymmetry 1. mathematical structure. J. Geophys. Res. 107 (A8), doi: 10.1029/2001JA000219.

Tsyganenko, N., 2002b. A model of the near magnetosphere with a dawn-dusk asymmetry 2. parameterization and fitting to observations. J. Geophys. Res. 107 (A8), doi: 10.1029/2001JA000220.

Tsyganenko, N., Singer, H., Kasper, J., 2003. Storm-time distortion of the inner magnetosphere: How severe can it get? J. Geophys. Res. 108(A5), doi:10.1029/2002JA009808.

Tsyganenko, N., Sitnov, M., 2005. Modeling the dynamics of the inner magnetosphere during strong geomagnetic storms. J. Geophys. Res. 110 A03108, doi:10.1029/2004JA010798.

Walton, D., Share, J., Rolph, T., Shaw, J., 1993. Microwave magnetisation. Geophys. Res. Let. 20, doi:10.1029/92GL02782.

Yang, S., Odah, H., Shaw, J., 2000. Variations in the geomagnetic dipole moment over the last 12000 years. Geophys. J. Int. 140, 158–162.

Table 1

Number of data used in CALS7K.2 by data types and components.

Type	Global	N Hemisphere	S Hemisphere
All	32353	27457	4896
All Decl.	13080	12254	826
All Incl.	16085	12182	3903
All Int.	3188	3021	167
Sediments	22953	18286	4667
Sediment Decl.	10637	9842	795
Sediment Incl.	12316	8444	3872
Sediment Int.	–	–	–
Archaeomag.	9400	9171	229
Archaeomag. Decl.	2443	2412	31
Archaeomag. Incl.	3769	3738	31
Archaeomag. Int.	3188	3021	167

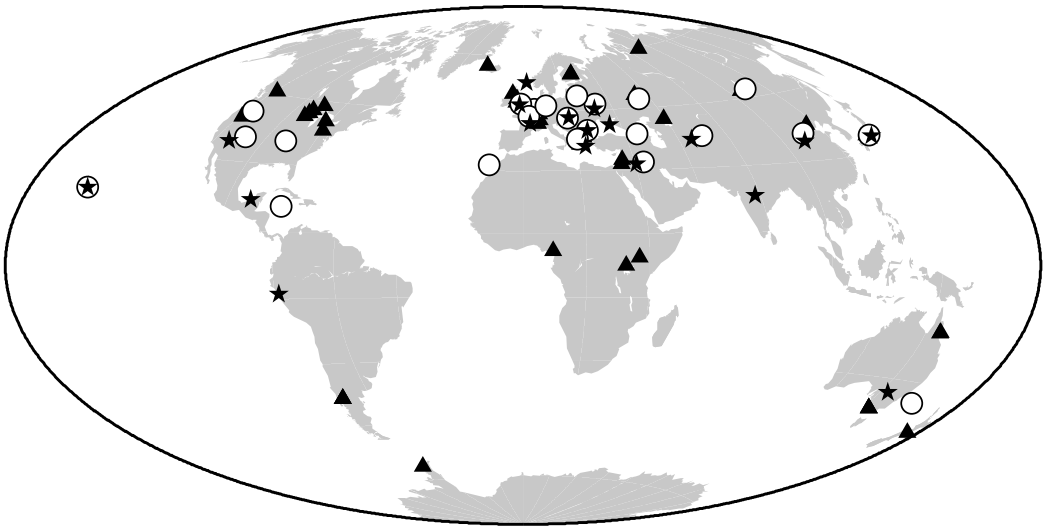

Fig. 1. Global data distribution for model CALS7K.2. Triangles are sediment sites, circles averages of regions with archaeomagnetic directional data, stars the same for archaeointensities.

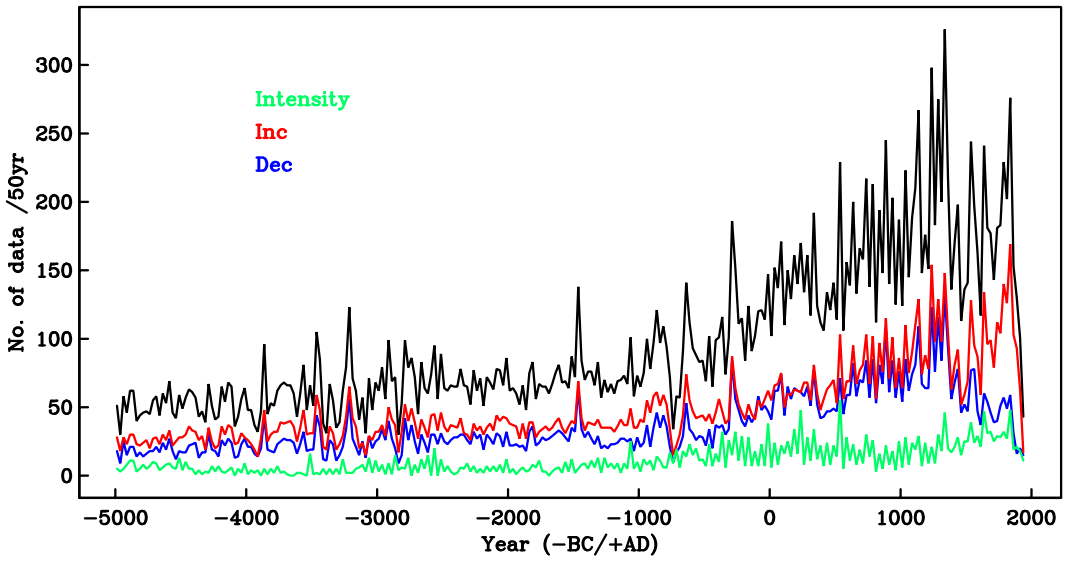

Fig. 2. Number of data per 50-year interval In black the total sum of the individual components inclination (red), declination (blue) and intensity (green).

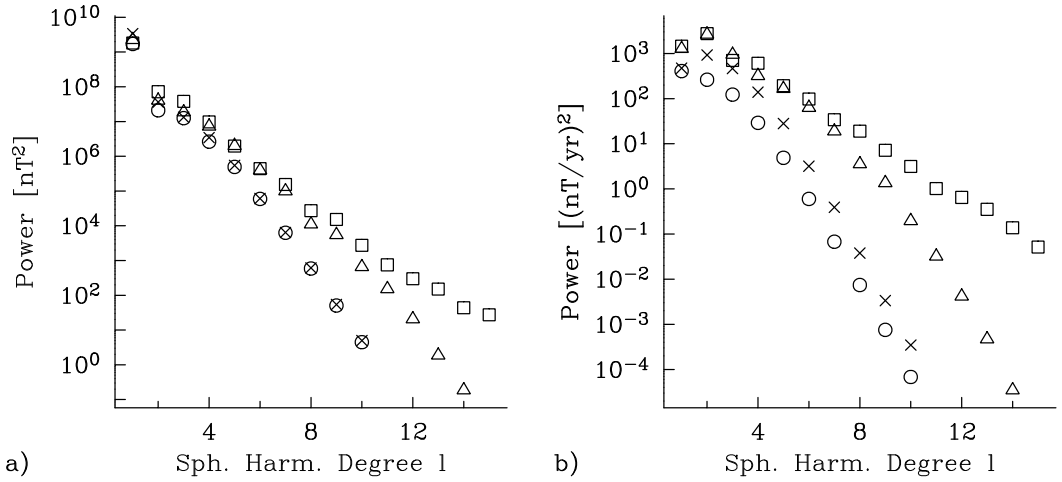

Fig. 3. Power spectra of magnetic field models (a) and their secular variation (b) at the Earth's surface: CALS7K.2 (circles), CALS3K.1 (crosses), GUFM (triangles, (Jackson et al., 2000)) and POMME1.4 (squares, (Maus et al., 2005))

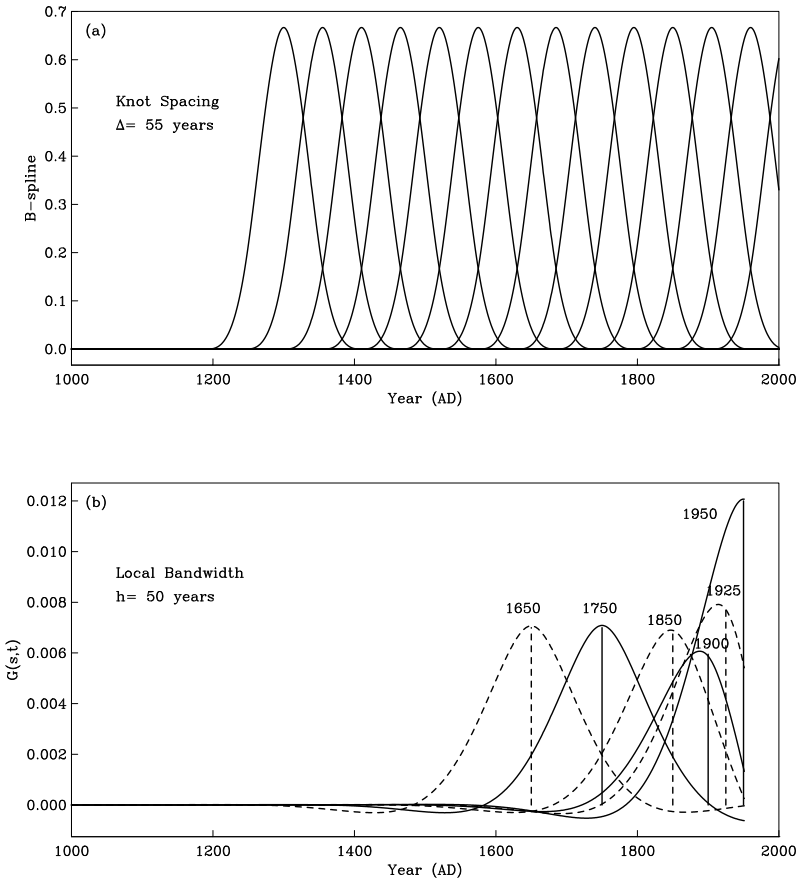

Fig. 4. (a) B-spline basis functions for a natural spline with knot spacing of 55 years. (b) Kernel function $G(s,t)$ with local bandwidth of $h = 50$ years. Vertical lines indicate the nominal time on which the kernel is centered. Note the asymmetry in G as one moves towards the end of the interval.

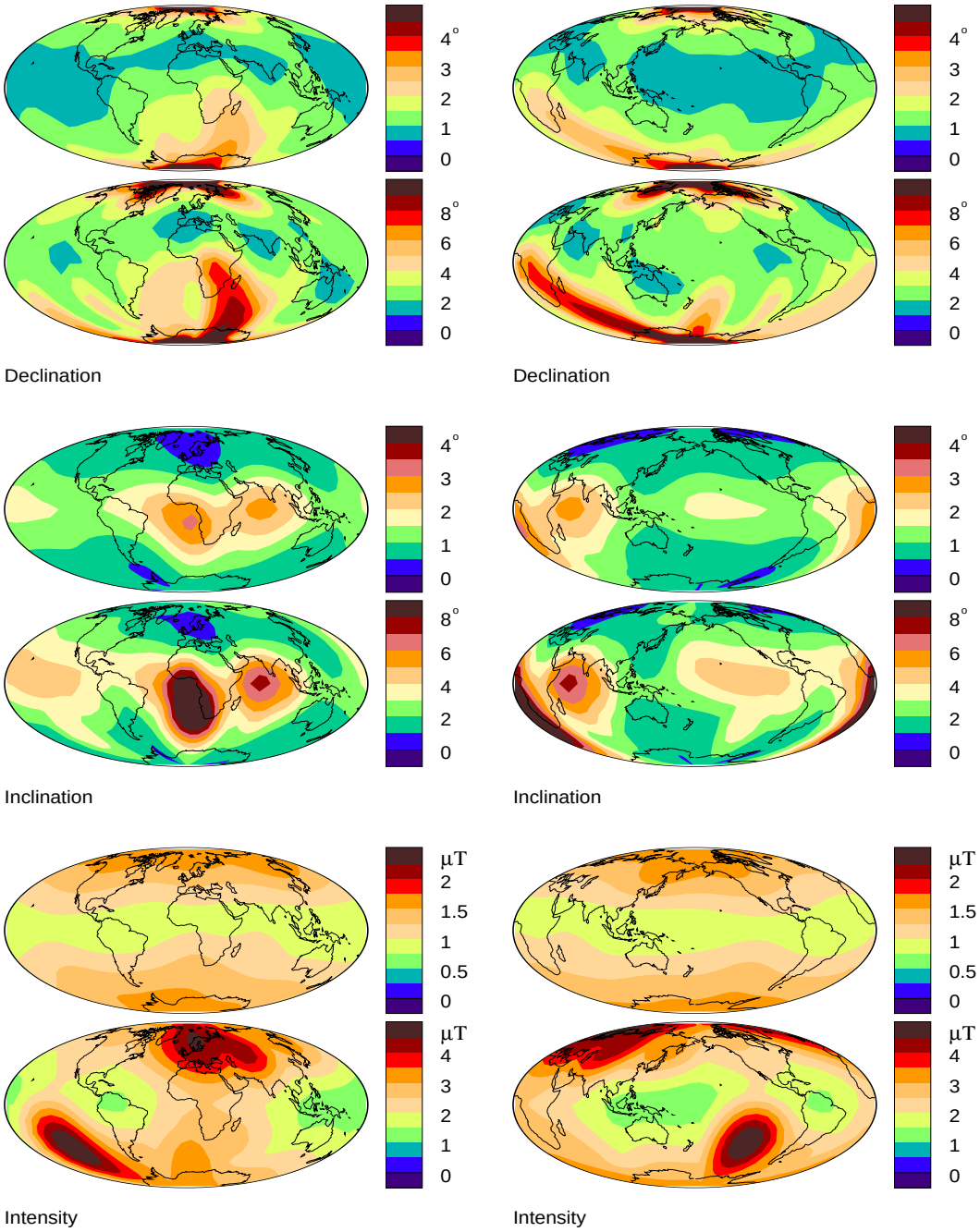

Fig. 5. Mean (top) and maximum (bottom) standard deviation in CALS7K.2 predictions over the whole time span of 7000 years in declination, inclination and intensity predictions. Note the different color scales for mean and maximum respectively. For convenience, the global maps are displayed centered both on longitude 0 and 180°.

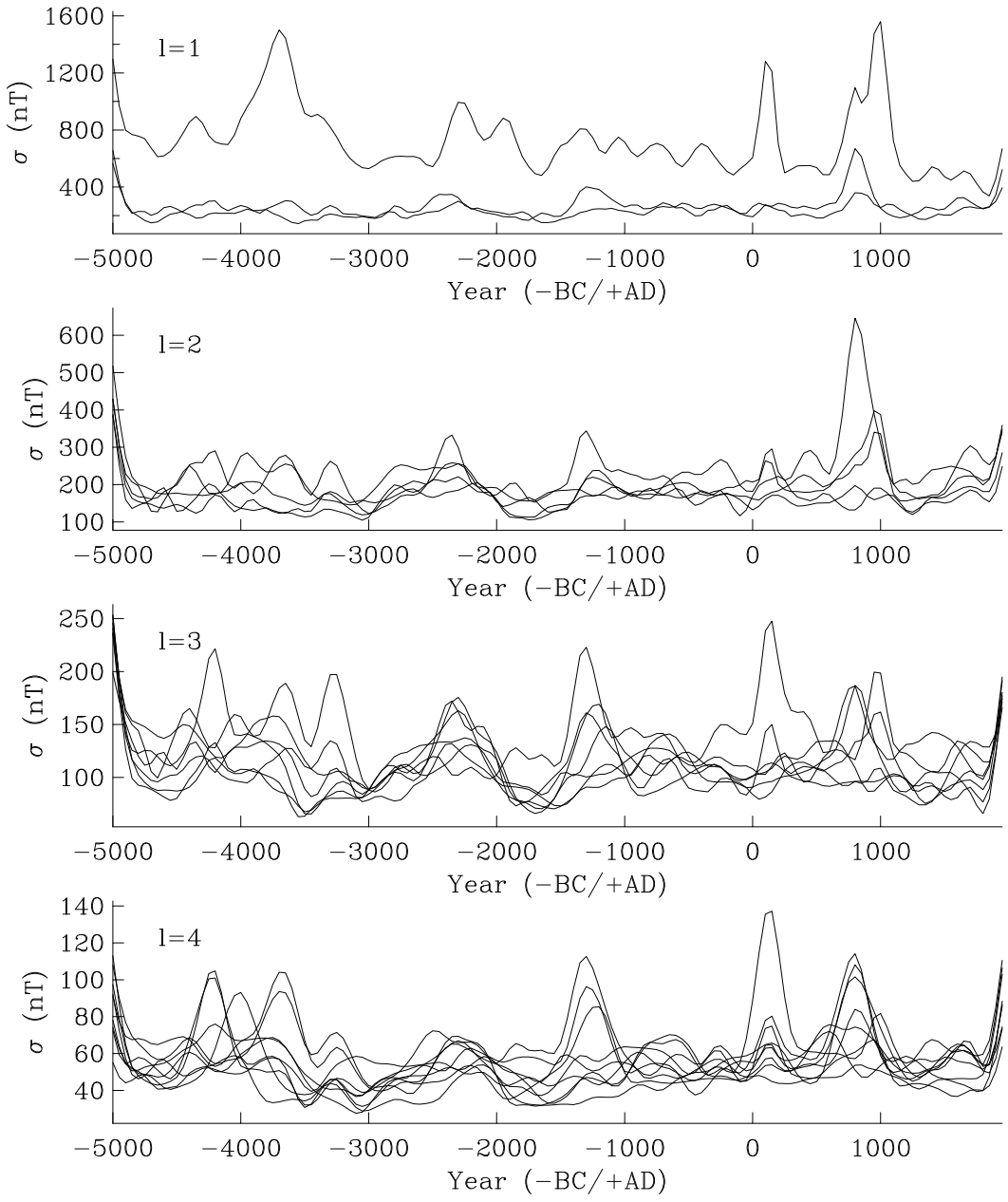

Fig. 6. Standard deviation in the individual coefficients with time for spherical harmonic degrees l=1 to 4. Uncertainties in the higher degree coefficients are similar to those in $l = 4$ with lower absolute values, corresponding to the lower high degree power.

.

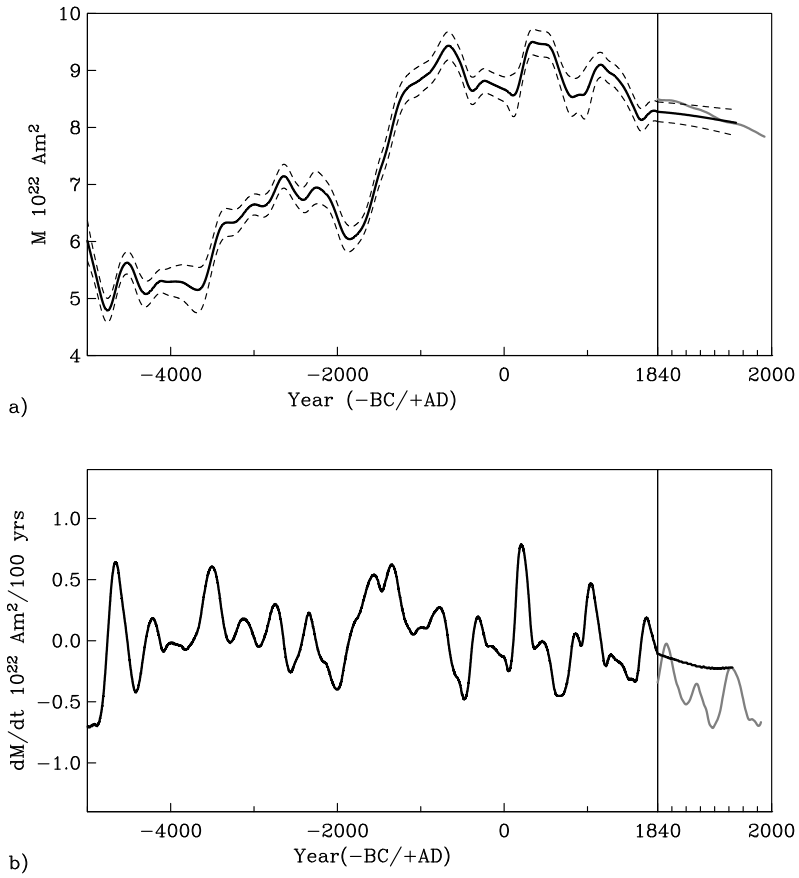

Fig. 7. CALS7K.2 dipole moment (a) and its derivative (b). In the extended right sections the same for GUFM (gray) is displayed for comparison. The uncertainty estimates (dashed lines) were obtained as standard deviation in moment evaluated for 3000 bootstrap models.

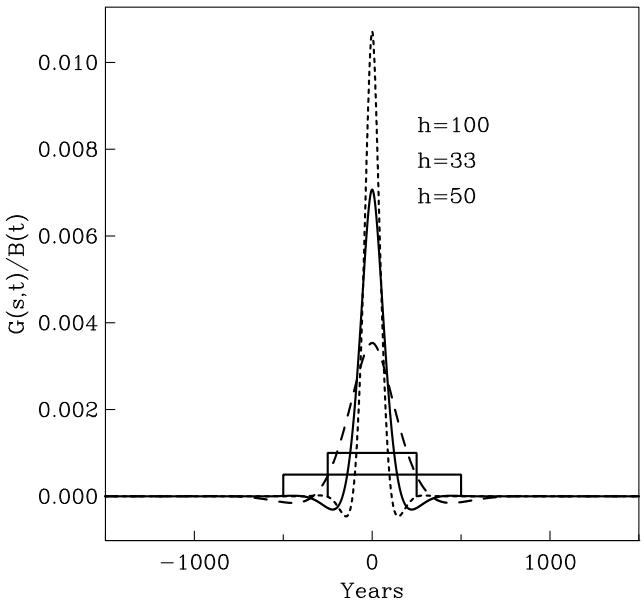

Fig. 8. Temporal averaging for 500 and 1000 year block averages $B(t)$, compared with spline kernels, G(s,t) of bandwidth $h = 33$ (short dashed line), 50 (solid), and 100 (long dashed) years. The average value of h for CALS7K.2 is about $h = 50$.

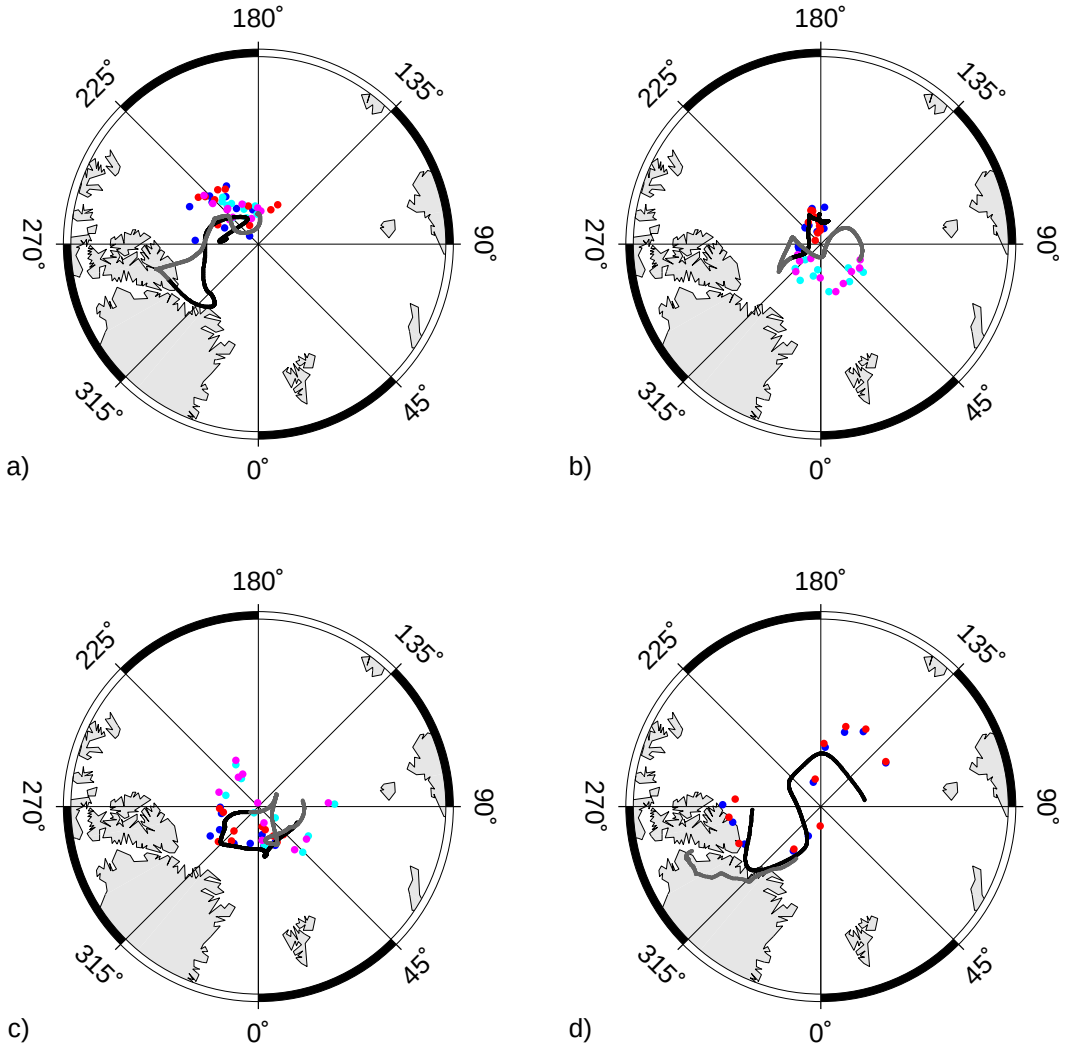

Fig. 9. Change of CALS7K.2 geomagnetic dipole position (black, gray), 100-year averaged VGPs from the data (blue, cyan) and from CALS7K.2 predictions (red, pink) with time. a) 5000 BC to 4000 BC (black,blue,red) and 4000 BC to 3000 BC (gray,cyan,pink), b) 3000 BC to 2000 BC (black,blue,red) and 2000 BC to 1000 BC (gray,cyan,pink), c) 1000 BC to 0 AD (black,blue,red) and 0 AD to 1000 AD (gray,cyan,pink) and d) 1000 AD to 1950 AD (black,blue,red) and GUFM prediction from 1590 to 1990 AD (gray).

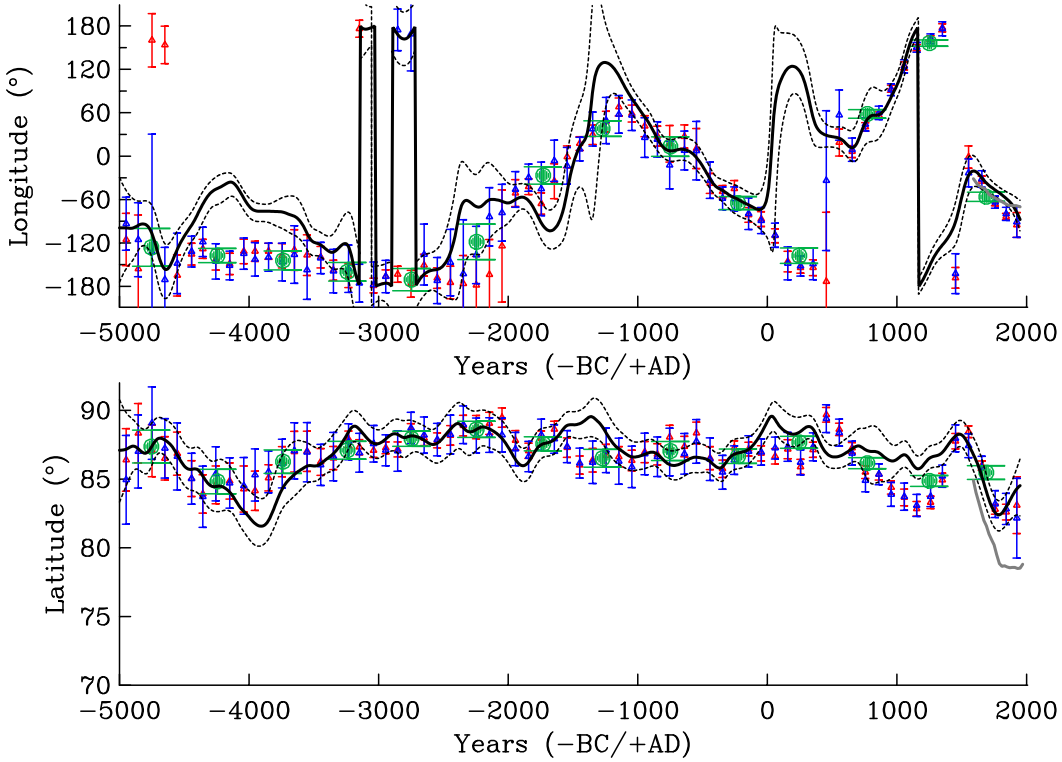

Fig. 10. Latitudinal (top) and longitudinal (bottom) change of geomagnetic pole position predicted from CALS7K.2 and GUFM (gray). Also shown are 100 year (blue) and 500 year (green) averages of VGP positions calculated directly from the data (D,I pairs), and 100 year averages of VGP predictions from CALS7K.2, along with their 95% confidence intervals.